Available online at BCREC website: https://bcrec.id

Bulletin of Chemical Reaction Engineering & Catalysis, 17 (3) 2022, 554-564

Research Article

Catalytic Dye Oxidation over CeO_2 Nanoparticles Supported on Regenerated Cellulose Membrane

Tran Thi Thuy[1], Dinh Ngoc Duong[1], Nguyen Quynh Vi[1], Nguyen Duc Duong[1], Tran Duc Thinh[1], Nguyen Cong Bang[1], Pham Hung Vuong[2], Nguyen Ngoc Mai[1,*]

[1]School of Chemical Engineering, Hanoi University of Science and Technology, No. 1 Dai Co Viet street, 10000 Hanoi, Vietnam.
[2]Advanced Institute for Science and Technology, Hanoi University of Science and Technology, No. 1 Dai Co Viet street, 10000 Hanoi, Vietnam.

Received: 3rd August 2022; Revised: 29th August 2022; Accepted: 30th August 2022
Available online: 10th September 2022; Published regularly: September 2022

Abstract

A novel regenerated cellulose (RC) membrane containing cerium oxide (CeO_2) nanoparticles is described in detail. In this work, CeO_2 nanoparticles with high surface area and mesoporosity were prepared by a modified template-assisted precipitation method. Successful synthesis was achieved using cerium nitrate as a precursor, adjusting the final pH solution to around 11 by ammonium hydroxide and ethylene diamine, and annealing at 550 °C for 3 hours under a protective gas flow. This resulted in a surface area of 55.55 $m^2.g^{-1}$ for the nanoparticles. The regenerated cellulose membrane containing CeO_2 particles was synthesized by the novel and environmentally friendly method. The catalyst CeO_2 and cellulose/CeO_2 membrane were characterized by Fourier transform infrared spectroscopy (FTIR), X-ray diffraction (XRD), Electron paramagnetic resonance (EPR), and Brunauer-Emmett-Teller (BET) measurements. The g-value of 2.276 has confirmed the presence of the surface superoxide species of CeO_2 nanoparticles in EPR. The photocatalytic activity of the catalyst and the membrane containing the catalyst was evaluated through the degradation of methylene blue under visible light irradiation by UV-VIS measurements. The cellulose/CeO_2 membrane degraded 80% of the methylene blue solution in 120 minutes, showing a better photocatalytic activity than the CeO_2 catalyst, which degraded approximately 62% in the same period. It has been proven that the RC membrane is not only a good transparent supporting material but also a good adsorption for high-performance of CeO_2 catalyst.

Keywords: Cellulose catalyst membrane; CeO_2 nanoparticles; regenerated cellulose membrane; wastewater treatment

How to Cite: T.T. Thuy, D.N. Duong, N.Q. Vi, N.D. Duong, T.D. Thinh, N.C. Bang, P.H. Vuong, N.N. Mai (2022). Catalytic Dye Oxidation over CeO_2 Nanoparticles Supported on Regenerated Cellulose Membrane. *Bulletin of Chemical Reaction Engineering & Catalysis*, 17(3), 554-564 (doi:10.9767/bcrec.17.3.15384.554-564)

Permalink/DOI: https://doi.org/10.9767/bcrec.17.3.15384.554-564

1. Introduction

Along with the remarkable development of industries worldwide, the environment is increasingly in danger when the amount of hazardous waste is generally increasing and exceeding the permissible threshold, including liquid waste. Wastewater from industries, especially the textile industry, contains many contaminants, which are dangerous to the ecosystem of aquatic species. These substances change most of the fundamental properties of water, such as high BOD, high pH values, and low percentage of oxygen in water, *etc.* [1]. If this problem is not addressed promptly, it will

* Corresponding Author.
Email: mai.nguyenngoc@hust.edu.vn (N.N. Mai);
Telp: +84-33-4032685

cause significant damage to the underwater ecosystem and cause severe environmental pollution. Protecting the environment and water resources from pollution problems are always the top concern of everyone.

Currently, there are four mainly and commonly used wastewater treatment methods: mechanical, physical-chemical, chemical, and biological. Nevertheless, no single method can thoroughly clean polluted water sources. The mechanical methods will remove coarse solid impurities from the wastewater with bars, garbage nets, *etc.* [2]. Physical-chemical methods such as coagulation/flocculation use other sedimentation aids to separate suspended particles from wastewater [3]. Both methods are applied individually or in combination but are only used to treat contaminated wastewater preliminarily. So, we must resort to chemical and biological methods to handle it more thoroughly. Currently, biological methods are more widely applied on a large scale to treat organic pigments in wastewater. However, this method suffers from the main disadvantage that microorganisms under anaerobic conditions can reduce azo dye into byproducts, which are toxic aromatic amines [4]. Chemical methods will change the characteristics of the wastewater [5]. Therefore, a new treatment direction has been studied, that is to treat pigments with advanced oxidation methods. The advanced oxidation method uses catalysts, which are semiconductors, to create free radicals or holes. When the semiconductors are illuminated, they generate $OH^{\bullet}$ (2.80 V) free radicals that are very powerful oxidizers and decompose most toxic organics [6].

Ceria is a cubic fluoride-type oxide that is considered as the most important rare-earth oxide. The most important applications of ceria are as catalysts and catalyst supports. This is because of excellent oxygen buffering properties and high tolerance to reversible oxygenation/deoxygenation cycles without disrupting the fluorite lattice-structure [7,8]. The use of cetyltrimethylammonium bromide (CTAB) for synthesizing high surface area CeO_2 nanoparticles with NaOH as a precipitating agent has been reported in the research [9]. However, the product can inevitably be contaminated with sodium. To deal with the problem, a precipitation solution consisting of ammonium hydroxide and ethylene diamine (EDA) could replace NaOH as a base. They play the same role as NaOH but will be removed entirely during heat treatment. With electron pairs at nitrogen atoms, NH_3 and EDA easily bind with metal ions (Ce^{3+}), especially bidentate EDA. The bidentate ligand EDA forms more stable metal complexes than those formed by a similar monodentate NH_3 ligand. The selection of EDA to control and slowly release Ce^{3+} creates a premise for the growth of $Ce(OH)_3$ precipitates. The controlling the precipitation rate of $Ce(OH)_3$ on the template assisted CTAB by using bidentate EDA would be a good condition for the growth of CeO_2 crystals during heat treatment [10,11]. It was found in the literature that the CeO_2 catalyst calcined in air at 500 °C was found to be able to decompose methylene orange up to 82.3% under visible light. To achieve the above effect, the appearance of oxygen vacancies on the surface is the main determining factor [12]. Therefore, the CeO_2-based catalyst synthesized from that precursor is expected to support a good photocatylic activity in the treatment of methylene blue.

Besides its tremendous efficiency, wastewater treatment with nano oxides has a disadvantage, namely the difficulty of recovering the catalyst after use [13,14]. Therefore, a support membrane was developed to prevent the catalyst from being washed away during the exposure process. Membranes used in water treatment technology are mostly synthetic polymer films such as polyvinylidene fluoride (PVDF), polysulfone (PSU), and poly vinyl chloride (PVC) [15–19]. These membranes are synthesized using a variety of chemicals. These processes can be environmentally harmful, and the membrane, after use is difficult to degrade. Moreover, environmental issues have taken on many new perspectives requiring treatment methods and sources of synthetic materials in studies to be environmentally friendly. Therefore, if criteria such as "renewability", "sustainability", "biodegradability" and "recyclability" are responded, the research materials will be able to apply more widely. Cellulose is a natural biomaterial that is widely used because it responds to most of the environmental friendliness criteria and low cost.

There are some common techniques for incorporating nanomaterials onto cellulose membranes, *e.g.* spraying catalyst solutions onto the membrane [20] or the impregnation method [21,22]. Studies demonstrate that the membrane surface is covered with a layer of photocatalytic nanoparticles in this approach. However, after a certain time, these photocatalysts are all washed away [23]. Therefore, this study aims to investigate the synthesis of RC membranes containing catalytic CeO_2 nanoparticles to oxidate

efficiently organic compounds. Herein, cellulose membranes are synthesized by the environmentally friendly method. Cellulose membranes serve as supports to ensure the dispersion and immobilization of catalysts during the work, while CeO_2 catalysts are responsible for the treatment of organic compounds in wastewater. The catalyst CeO_2 and cellulose/CeO_2 membrane were characterized by Fourier transform infrared spectroscopy (FTIR), X-ray diffraction (XRD), Electron paramagnetic resonance (EPR), Brunauer-Emmett-Teller (BET), and UV-DRS (Ultraviolet-Visible Diffuse Reflectance Spectroscopy) measurements. The photocatalytic activity of the catalyst and the membrane containing the catalyst was evaluated through the degradation of methylene blue (MB) under visible light irradiation by UV-VIS measurements.

2. Materials and Methods

2.1 Materials

Cerium nitrate ($Ce(NO_3)_3.6H_2O$, 99.5%) and tetrabutylphosphonium hydroxide (TBPH) containing 40 wt% in water were purchased from Acros. Microcrystalline cellulose (MCC) with the size 20 µm and methylene blue (MB) used in this study were purchased from Sigma Aldrich. Propylene carbonate (PC, 99.7%), dimethyl sulfoxide (DMSO, 99.9%), cetyltrimethylammonium bromide (CTAB, >99%), and ethylenediamine (EDA, ≥99.5%) were obtained from Sigma Aldrich. Sodium hydroxide (NaOH) and ammonium hydroxide (NH_4OH) were purchased from Acros.

2.2 Methods

2.2.1 Synthesis of catalyst CeO_2

Schematic overview of CeO_2 synthesis using the template-assisted precipitation method is shown in Figure 1. CeO_2 precursors were prepared by dissolving $Ce(NO_3)_3.6H_2O$ and CTAB in water with the stoichiometric ratio Ce^{3+}:CTAB of 1:0.6. To promote precipitation, the solution included NH_4OH and EDA was added to the CeO_2 precursors, whose pH was adjusted to around 11. This solution was precipitated for 16 h in the temperature range from 90 to 100 °C. The yellow precipitates were then dried at 100 °C for 6 h and continued to calcine under inert gas at 550 °C for 3 h.

2.2.2 Synthesis of cellulose/CeO_2 composite membrane

A composite membrane between CeO_2 nanoparticles and RC membrane was prepared by

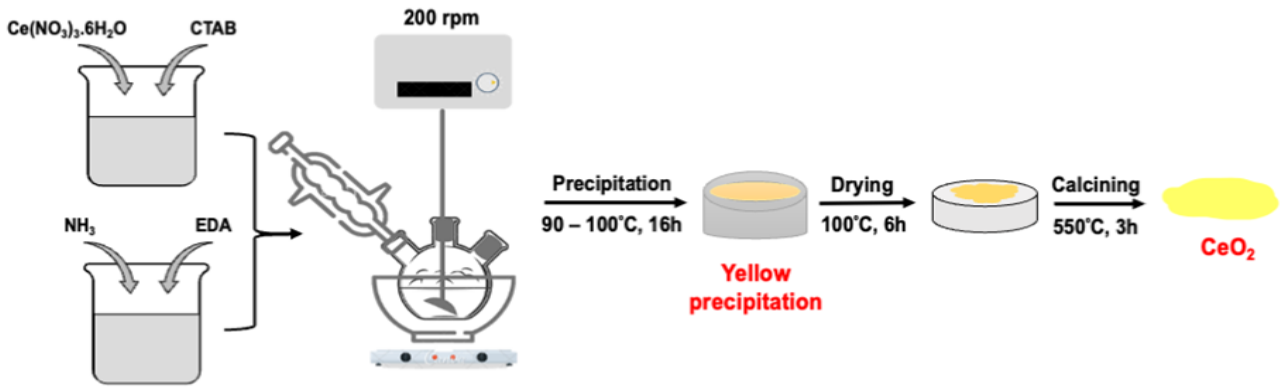

Figure 1. Schematic overview of CeO_2 synthesis using template-assisted precipitation method.

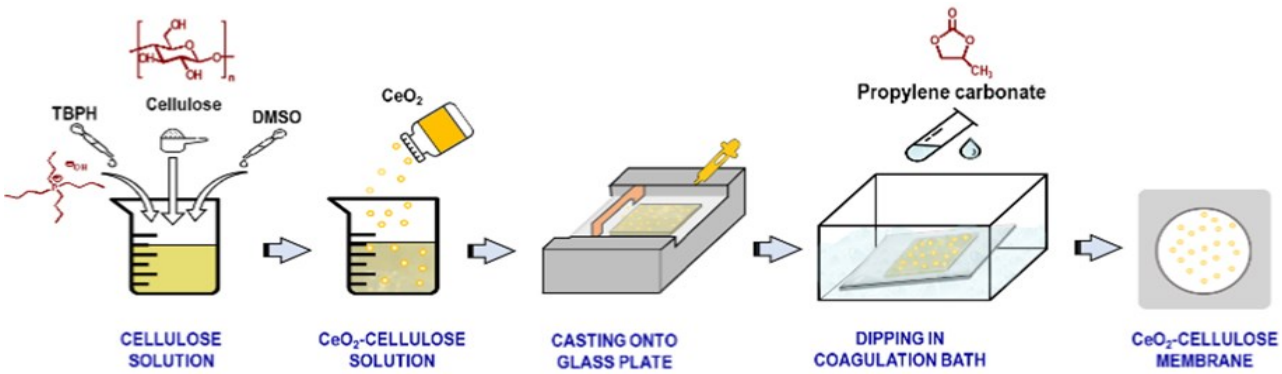

Figure 2. Synthesis of cellulose/CeO_2 composite membrane.

dispersing the nanoparticles in the cellulose casting solution (Figure 2).

First, cellulose needs to be dissolved in TBPH to obtain a clear and homogeneous solution. TBPH 40 wt% was condensed to a higher concentration of TBPH 50 wt% by using rotary evaporation at 60 mbar under 40 °C. Microcrystalline cellulose (200 mg, 20 wt%) was dissolved in TBPH (1 mL of 50 wt% in water) and DMSO (0.35 mL) at room temperature (25 °C). After 30 minutes of stirring at 300 rpm, the corresponding weight of CeO_2 was added. The cellulose nanomaterials suspension was cast onto a glass plate with a defined thickness of 500 μm. The cast liquid film was rapidly immersed in a propylene carbonate bath for coagulation and was washed with deionized water to obtain a homogeneous membrane.

2.2.3 Investigation of the photocatalytic performance of catalyst powder and RC/catalyst membrane

The photocatalytic ability of the catalyst powder, cellulose membrane and RC/catalyst membrane was evaluated by the degradation of MB at 5 ppm. For the evaluation of catalyst, samples of 0.01 g CeO_2 powder were taken and added to 50 mL of the prepared MB solution. First, the MB solution containing the catalyst was stirred in the dark for 40 min to allow complete absorption of the catalyst samples. Then, the solution was stirred under a light source for two hours. The light source used in this study was a xenon lamp (300 W), which provides visible radiation. The photocatalytic ability of the membrane containing the same amount of CeO_2 and the cellulose membrane were tested using the same procedure. A sample of the solution was taken every 20 min and all catalysts were removed by centrifugation.

The concentration of MB solution was analyzed by recording the absorbance at 664 nm using Avantes UV-Vis spectrometer. The concentration of MB solution is determined through a calibration curve when its absorbance value is known. The principles of this method follow the Lambert-Beer law:

$$A = \log\left(\frac{I_0}{I}\right) = \varepsilon c L \tag{1}$$

where, I_0 is the incident intensity, I is the transmitted intensity, the quantity ε is the molar absorptivity (or extinction coefficient), and L is the path length. Molar absorptivity is the property of a substance that indicates how much light is absorbed in each wavelength.

The degradation efficiency of MB can be calculated according to the following formula:

$$Degradation\ efficiency(\%) = \frac{[MB]_{inlet} - [MB]_{outlet}}{[MB]_{inlet}} \times 100 \tag{2}$$

where, $[MB]_{inlet}$ represents the concentration of MB in the feeding stream (ppm) and $[MB]_{outlet}$ is the concentration of MB in the outlet stream (ppm).

2.3 Characterization

Fourier transform infrared spectroscopy (FTIR) of samples was measured with a Nicolet iS50 FTIR (Thermo Fisher Scientific) in Attenuated total reflection (ATR) mode. The specimens were investigated directly with a scan range from 500 to 4000 cm^{-1}. X-ray diffraction (XRD) powder pattern was recorded in the 2θ range from 10–80° by X'Pert Pro equipped (PANalytical) equipped with an X'Celerator RTMS Detector under condition Cu Kα radiation (40 kV, 35 mA). The morphologies of catalyst were characterized by Field emission scanning electron microscopy (FE-SEM) on a Hitachi S4800 instrument. The specimen was measured at an accelerating voltage of 5 kV with a 5 nm platinum coating using an ion sputter (E-1020, Hitachi High Technologies). The transmission electron micrograph (TEM) observation was performed with a JEOL ARM200F instrument equipped with a JED-2300 energy-dispersive X-ray spectrometer (EDXS) for chemical analysis. The surface and mapping measurements were recorded by scanning electron microscopy-energy dispersive X-ray spectroscopy NeoScope JCM-7000 (JEOL) benchtop SEM. The sample's surface area, pore volume, and pore diameter were measured via N_2 adsorption/desorption isotherms using the Brunauer-Emmett-Teller (BET) method on a Micromeritics Gemini VII 2390 analyzer. Electron paramagnetic resonance (EPR) spectra were recorded with a continuous wave X-band by Bruker EMX-Micro EPR spectrometer with a microwave power of 1.976 mW, frequency 9.410 GHz, modulation frequency 100 kHz and amplitude 5 G at 100 K, the magnetic field was full range from 100 to 6500 G. The UV-Vis spectra of the samples were obtained using an Avantes UV-Vis spectrometer. This method shows the concentration of methylene blue solution before and after the photocatalytic process.

3. Results and Discussion

3.1 Characterization of Catalyst CeO_2 and Cellulose Catalyst Membrane

The FTIR spectrums of CeO_2 nanoparticles, cellulose membrane, and cellulose membrane containing catalyst CeO_2 are shown in Figure 3. These spectra of cellulose membrane and cellulose/CeO_2 membrane show that cellulose I has completely transformed into cellulose II after the coagulation [24]. The broad bands which are centered at 3318 and 3328 cm^{-1} are attributed to the O−H stretching vibrations, while the absorption bands at 2892 and 2894 cm^{-1} are CH_2. The bands at 1643 and 1645 cm^{-1} are due to the scissor bending mode of associated water. Typical bands assigned to cellulose materials at 1159 and 895 cm^{-1} are due to C−O−C stretching at the β-(1→4)-glycosidic linkages. In the spectrum of CeO_2 nanoparticles, the absorption bands at 3384, 1633, 1301, 977, and 865 cm^{-1} are attributed to the stretching mode of water and hydroxyl groups. The peak at 510 cm^{-1} corresponds to the asymmetric O−Ce−O stretching mode of vibration. Due to minor changes, it is assumed that CeO_2 nanoparticles have no effect on the FTIR spectrum of the cellulose membrane. On the other hand, the received signals in the 510 cm^{-1} wavelength range were not very clear, so other analyzes were performed to better understand the structure of the catalyst and the membrane.

Figure 4 exhibits the XRD pattern of CeO_2 nanoparticles and CeO_2 nanoparticles dispersed in the cellulose membrane. The well-resolved peaks in XRD can be accurately attributed to the pure cubic fluorite structure. As can be seen in the Figure 4, the strong CeO_2 (200) at 33.1° and absence of non-(h00) peaks indicated that the CeO_2 nanoparticles have a strong cube texture. The synthesized cellulose / CeO_2 membrane showed the different diffraction reflections at 2θ = 20.6° (a primary 101 reflection overlapping with a reduced 002 reflection). It corresponds mainly to cellulose II. Thus, the XRD measurements of the cellulose/CeO_2 membrane indicate a conversion of cellulose I to cellulose II that occurs during the process of membrane formation [24,25]. However, the characteristic peak of CeO_2 remains. This proves that having successfully synthesized and applied cerium oxide to the cellulose membrane, the crystal structure of CeO_2 is preserved. This is a favorable premise for MB decomposition of cellulose/CeO_2 membrane. The average crystalline size of CeO_2 nanoparticles was 3.85 nm, calculated according to Debye's Scherrer equation.

The cellulose membrane containing cerium oxide catalyst obtained after synthesis by the coagulation method was evaluated for its morphology by SEM analysis (Figure 5(A)). The surface of the regenerated cellulose membrane appears very smooth, dense, and uniform [24]. In contrast, the added CeO_2 made the film rough and uneven. However, the synthesized catalyst particles are distributed quite uniformly throughout the surface of the membrane (Figure 5(B)). The uniform distribution of catalysts on the membrane brings good efficiency to using catalytic membranes for wastewater treatment. Specifically, when the organic dyes in the wastewater pass through the membrane, they will be exposed to many catalytic nanoparticles and be treated more thoroughly.

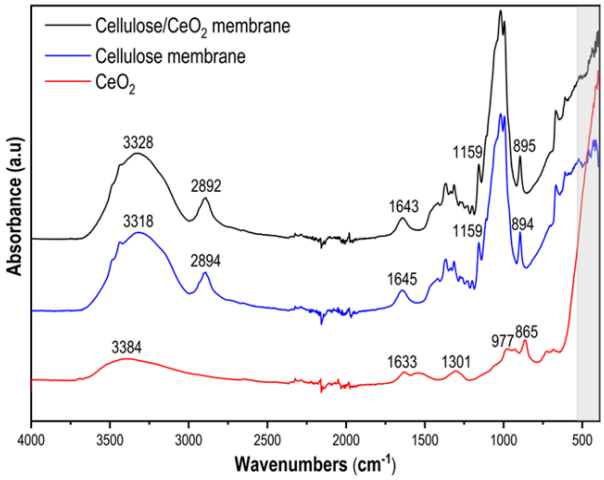

Figure 3. FTIR spectrum of CeO_2, cellulose membrane, and cellulose/CeO_2 membrane.

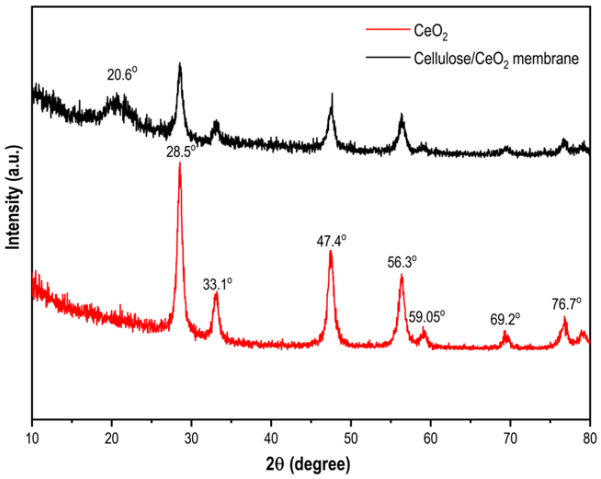

Figure 4. XRD pattern of the annealed CeO_2 nanoparticles and cellulose/CeO_2 membrane.

The morphologies of the annealed CeO_2 samples were investigated through FE-SEM images. Figure 6(A) displays a representative overview of the straw-like CeO_2 nanostructures, which shows that the obtained products are composed entirely of large-scale thin rod-like structures. It is found that large numbers of thin rod-like CeO_2 were chaotic stacking. A tiny minority of nanotubes paralleled flocked together with high density were attached tightly along with their nanoparticle forms, resulting in enormous holes as shown in Figure 6(B). The diameter of rod-like structures is 20 to 30 nm, and their lengths vary from 250 to 300 nm. As previously mentioned in the XRD results, an increase in the calcination temperature results in improved crystallinity of CeO_2 because of the removal of the impurities from CeO_2 [26].

The morphologies of CeO_2 samples were also examined by TEM. As presented in Figure 7, the dark domain may be identified as CeO_2. The annealed CeO_2 at 550 °C has a crystalline size varying from 3 to 5 nm. The pore size was above 3 nm, covered by CeO_2. It agrees with the above XRD assignment, thus the cubic fluorite structure of CeO_2 is supported. CeO_2 nanoparticles have polyhedron morphology, showed by a red circle in Figure 7(A). The outer surface of the shells is composed of many small particles. These tiny particles are disorder aggregation by the analysis of lattice fringes as seen in Figure 7(B). The crystal planes are overlapped as it is displayed in Figure 7(C). It indicates the polycrystalline character of CeO_2 nanoparticles, and the majority of the hierarchical structures vanish fully while the largescale nanorod/nanotube blends are gotten. In Figure 7(D), the building blocks of CeO_2 hierarchical architectures have a cubic fluorite structure.

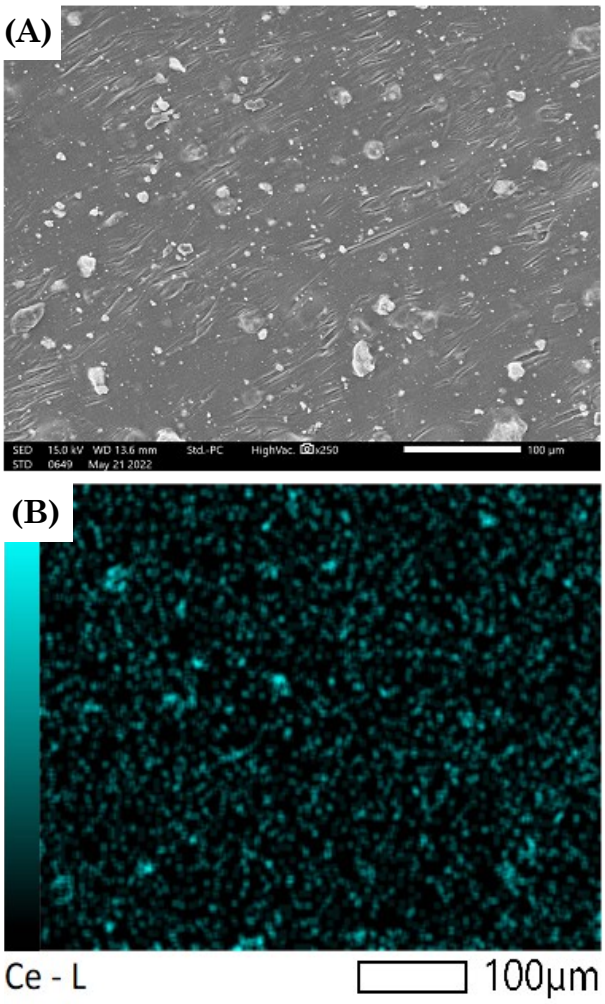

Figure 5. (A) Cellulose/CeO_2 membrane surface structure and (B) Mapping of membrane for elemental compositions.

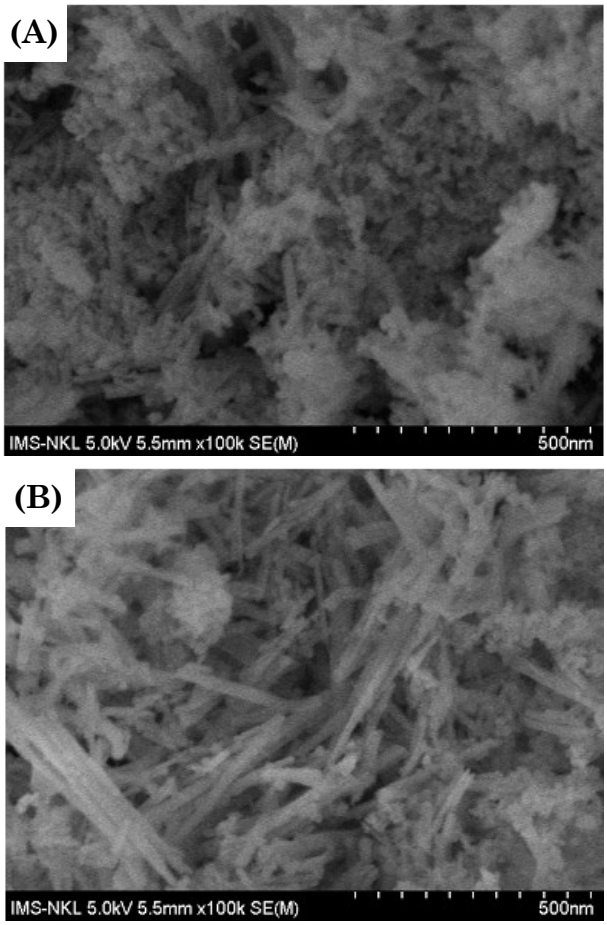

Figure 6. FE-SEM micrographs of the annealed CeO_2 nanoparticles at 550 °C.

The attendance of oxygen vacancies in cerium oxide nanoparticles can be examined by electron paramagnetic resonance spectroscopy (EPR). Figure 8 shows the EPR spectrum of CeO_2 nanoparticles recorded at 100 K and g = 2.276, indicating the presence of the surface superoxide species. O• radicals are generated through the redox of Ce^{3+}/Ce^{4+} according to the following equation:

$$e^- + CeO_2\ (Ce^{4+}) \rightarrow CeO_2\ (Ce^{3+}) \quad (3)$$

$$O_2^- + h^+ \rightarrow O^{\bullet -} \quad (4)$$

Both the OH• radical formed on the catalyst surface and the $O^{\bullet -}$ radical cause oxidative degradation of organic pigments. The obtained EPR image with the g-value is consistent with the characteristics of the CeO_2 nanoparticles.

To further explore the detailed structure of the CeO_2 catalyst, N_2 adsorption-desorption

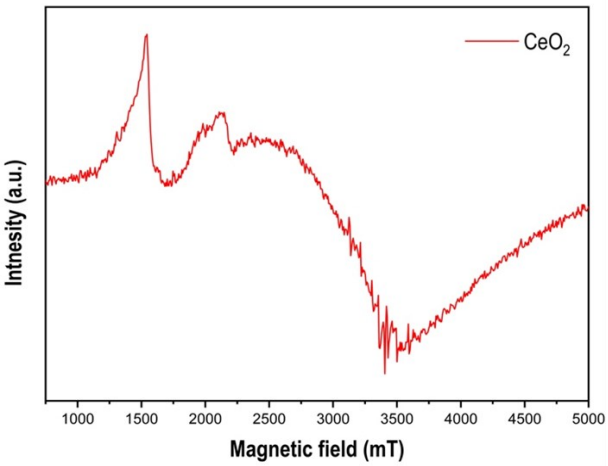

Figure 8. EPR spectrum of the annealed CeO_2 nanoparticles at 550 °C.

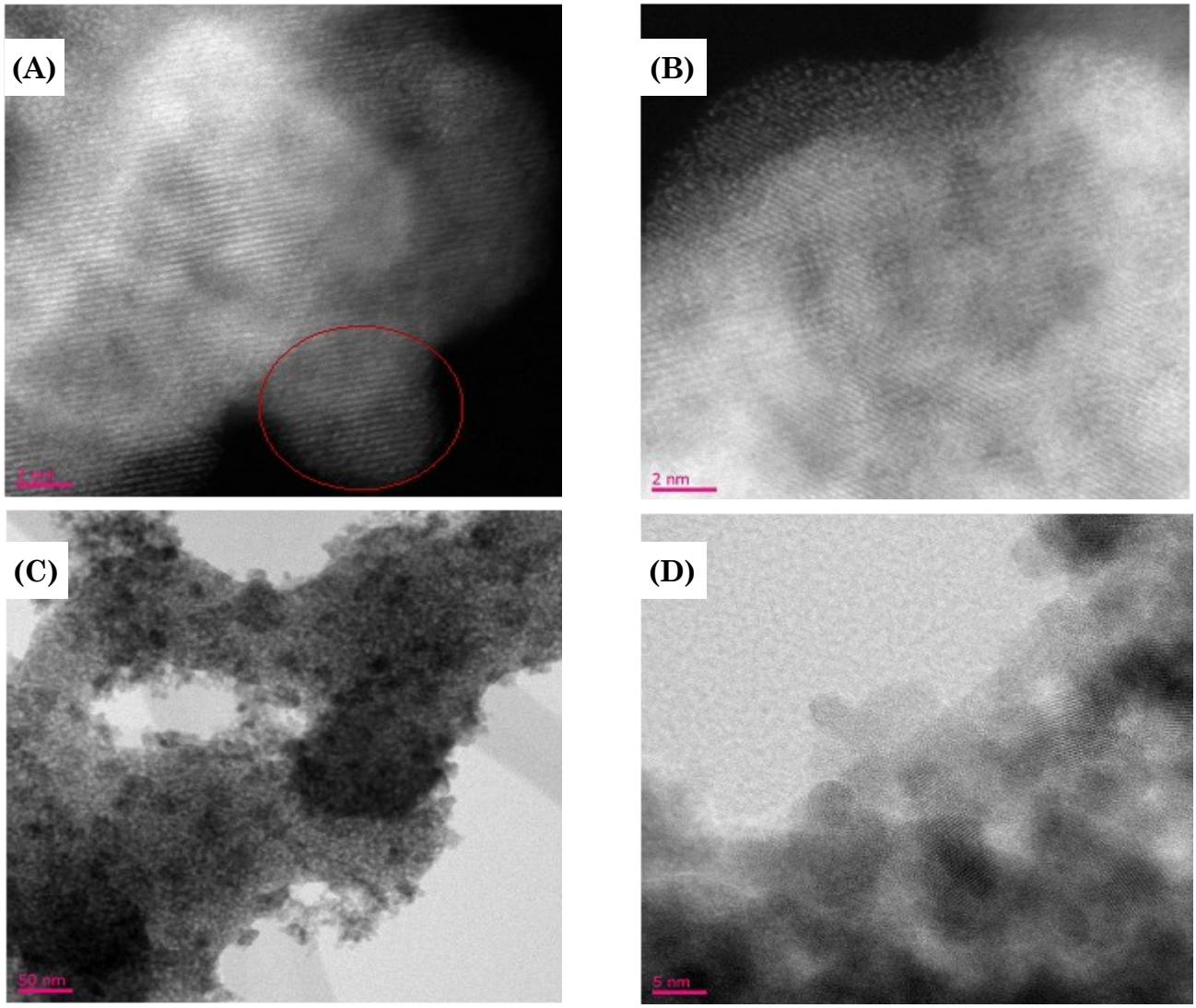

Figure 7. TEM micrographs of CeO_2 nanoparticles synthesized at 550 °C at different magnifications.

Joyner-Halenda (BJH) pore size distributions were employed to determine the pore area and specific pore volume (Figure 9). In Figure 9(A), the sample exhibited isotherm of type IV (Brunauer-Deming-Deming-Teller BDDT classification) with type H3 hysteresis loops in the relative pressure range of 0.75–1, indicating the presence of mesoporous structure. Brunauer-Emmett-Teller (BET) surface area analysis gave a value of 55.5464 $m^2.g^{-1}$. The corresponding pore size distribution of the sample is shown in Figure 9(B). The pore size distribution is mainly concentrated at 28.96 nm.

3.2 Evaluation of the Activity of Catalyst CeO_2 and Cellulose Catalyst Membrane

The bandgap energy of the synthesized CeO_2 sample has the value E_g = 2 eV (Figure 10(B)). This result indicates that the synthesized catalyst has the potential to enhance adsorption under visible light. However, as announced by Jiang [27], E_g has a value that CeO_2 can absorb visible radiation but no electronic transition occurs. The explanation for the measured results is that the significant appearance of Ce^{3+} (Ce_2O_3) in the catalytic sample in the presence of an electron in the 4f quantum cell easily excites the transition to a higher energy level [28]. Moreover, based on the EPR result, the presence of oxygen vacancies on the material is a favorable condition for the movement of free electrons. This allows the electrons to escape more easily, resulting in a low E_g value. Therefore, the bandgap value of the synthesized CeO_2 sample has the same value as mentioned above.

The photocatalytic activity of the CeO_2 catalyst and cellulose/CeO_2 membrane was evaluated by the ability to decompose methylene blue (MB) under visible light. The

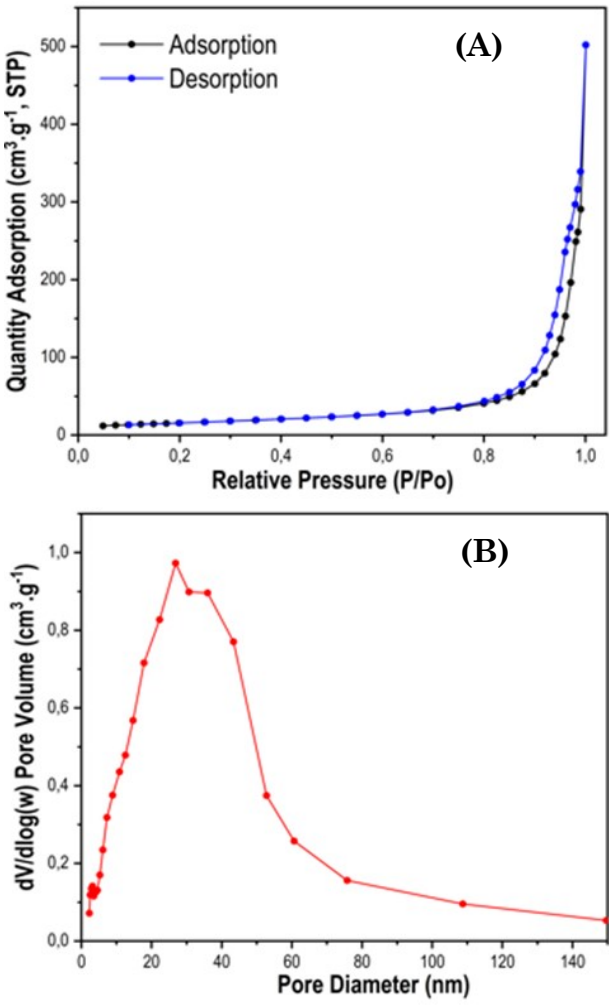

Figure 9. The quantity adsorbed as a function of relative pressure (isotherm liner plot) of the CeO_2 sample (A) and BJH distribution of CeO_2 (B).

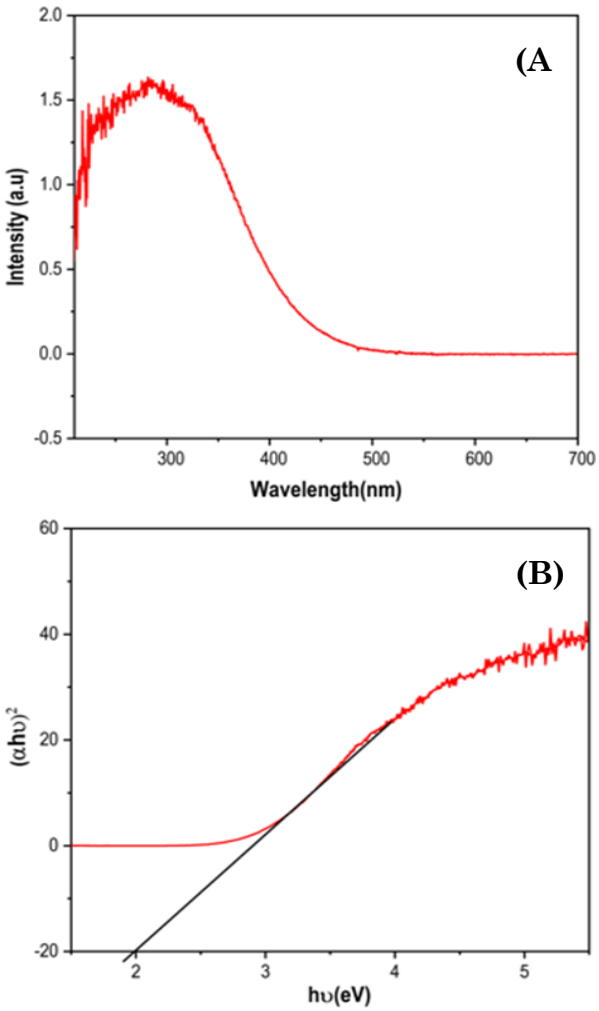

Figure 10. (A) UV-DRS spectrum of CeO_2, (B) The tauc graph calculates the bandgap energy.

influence of the membrane on the catalytic activity was also considered here (Figure 11).

In Figure 11(A), the photocatalytic activity of the cellulose/CeO_2 membrane is better than that of the CeO_2 catalyst. The cellulose/CeO_2 membrane degraded nearly 80% of the MB solution in 120 min, while the CeO_2 catalyst degraded approximately 62% in the same period. This shows that the RC membrane does not block light and affects the quality of the photocatalyst. Besides, the ability to treat pigments of cellulose membrane was also evaluated. After 40 min without light, the equilibrium of the regenerated cellulose membrane was reached at 53.2% in the adsorption processes. This reason can be explained that the cellulose membrane could absorb the color of the solution due to a negative zeta potential of the membrane [24], so the concentration of MB in the solution is also significantly reduced. When light on, the degradation efficiency of cellulose membrane did not change. This result shows that MB was completely adsorbed onto the cellulose membrane and the cellulose membrane was unable to treat the organic dye. In addition, the uniform distribution of catalyst particles on the membrane increased the catalytic efficiency.

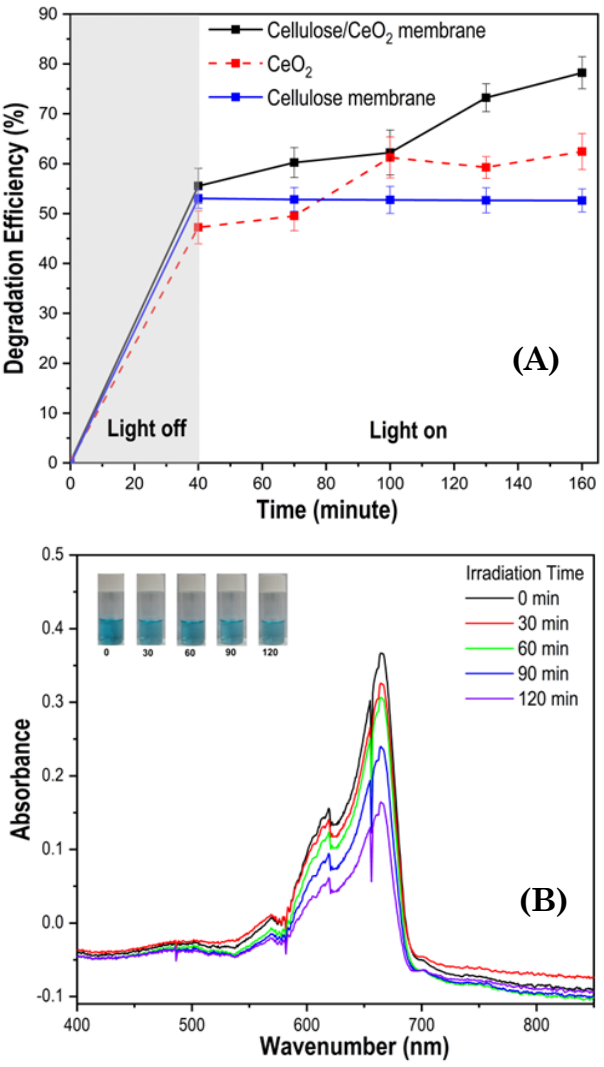

Figure 11. Photoactivity of catalyst CeO_2, cellulose membrane and cellulose/CeO_2 membrane.

Figure 11(B) shows the UV-Vis spectrum of the cellulose/CeO_2 membrane. The color of the MB changed after being illuminated with a xenon lamp for 120 min. The absorbance (A) of the solution decreased from 0.426 to 0.232, corresponding to a decrease in the concentration of MB from 2.235 ppm to 1.133 ppm. The above results show great potential as a photocatalyst to decompose wastewater treatment for the textile industry.

4. Conclusions

The CeO_2 nanoparticles were successfully synthesized using the template-assisted precipitation technique with high surface area and mesoporosity. In addition, the catalyst sample was easily incorporated into the regenerated cellulose membrane using non-toxic chemicals and a simple procedure. The photocatalyst as well as the composite membrane were characterized by FT-IR, XRD, and UV-vis spectroscopy. Their morphologies were studied by FE-SEM and TEM. The annealed CeO_2 at 550 °C has a crystalline size varying from 3 to 5 nm. This novel method has been demonstrated to be highly effective for the immobilization and distribution of catalysts inside the membrane. The photocatalytic cellulose/CeO_2 membrane was applied effectively in wastewater treatment due to RC membrane's sustainability as well as the strong oxidation capacity of the photocatalyst. The membrane showed good MB elimination performance under visible radiation, degrading nearly 80% of the MB solution in 120 min. It has shown great potential to be used in photocatalytic membrane reactors for the degradation of wastewater treatment in the textile industry.

Acknowledgment

This research was supported by Kurita Asia Research Grant (21Pvn012-45R) provided by Kurita Water and Environment Foundation and RoHan Project funded by the German Academic Exchange Service (DAAD, No. 57315854) and the Federal Ministry for Economic Cooperation and Development (BMZ) inside the framework "SDG Bilateral Graduate School Programme".

References

[1] Bhatia, S.C. (2017). *Pollution control in textile industry*. New York: WPI Publishing.

[2] Bhargava, D.A. (2016). Physico-Chemical Waste Water Treatment Technologies: An Overview. *International Journal Of Scientific Research And Education*, 4(5), 5308–5319. DOI: 10.18535/ijsre/v4i05.05.

[3] Meriç, S., Selçuk, H., Belgiorno, V. (2005). Acute toxicity removal in textile finishing wastewater by Fenton's oxidation, ozone and coagulation-flocculation processes. *Water Research*, 39(6), 1147–1153. DOI: 10.1016/j.watres.2004.12.021.

[4] Abdel-Shafy, H.I., Mansour, M.S.M. (2016). A review on polycyclic aromatic hydrocarbons: Source, environmental impact, effect on human health and remediation. *Egyptian Journal of Petroleum*, 25(1), 107–123. DOI: 10.1016/j.ejpe.2015.03.011.

[5] Butani, S.A., Mane, S.J. (2017). Coagulation / Flocculation Process for Cationic, Anionic Dye Removal Using Water Treatment Residuals – A Review. *International Journal of Science Technology and Management*, 6(4), 1–5.

[6] Sharma, S., Ruparelia, J., Patel, M. (2011). A general review on advanced oxidation processes for waste water treatment. *Institute of Technology Nirma University Ahmedabad*, 481, 8–10.

[7] Montini, T., Melchionna, M., Monai, M., Fornasiero, P. (2016). Fundamentals and Catalytic Applications of CeO_2-Based Materials. *Chemical Reviews*, 116(10), 5987–6041. DOI: 10.1021/acs.chemrev.5b00603.

[8] Zhang, S., Wang, H., Si, H., Jia, X., Wang, Z., Li, Q., Kong, J., Zhang, J. (2020). Novel Core-Shell (ϵ-MnO_2/CeO_2)@CeO_2 Composite Catalyst with a Synergistic Effect for Efficient Formaldehyde Oxidation. *ACS Applied Materials and Interfaces*, 12(36), 40285–40295. DOI: 10.1021/acsami.0c09263.

[9] Yuejuan, W., Jingmeng, M., Mengfei, L., Ping, F., Mai, H. (2007). Preparation of High-Surface Area Nano-CeO_2 by Template-Assisted Precipitation Method. *Journal of Rare Earths*, 25(1), 58–62. DOI: 10.1016/S1002-0721(07)60045-3.

[10] Thuy, T.T., Hoste, S., Herman, G.G., Van de Velde, N., De Buysser, K., Van Driessche, I. (2009). Novel water based cerium acetate precursor solution for the deposition of epitaxial cerium oxide films as HTSC buffers. *Journal of Sol-Gel Science and Technology*, 51(1), 112–118. DOI: 10.1007/s10971-009-1949-7.

[11] Thuy, T.T., Lommens, P., Narayanan, V., Van de Velde, N., De Buysser, K., Herman, G.G., Cloet, V., Van Driessche, I. (2010). A nitrilo-tri-acetic-acid/acetic acid route for the deposition of epitaxial cerium oxide films as high temperature superconductor buffer layers. *Journal of Solid State Chemistry*, 183(9), 2154–2160. DOI: 10.1016/j.jssc.2010.07.009.

[12] Fauzi, A.A., Jalil, A.A., Hassan, N.S., Aziz, F.F.A., Azami, M.S., Hussain, I., Saravanan, R., Vo, D.-V.N. (2022). A critical review on relationship of CeO_2-based photocatalyst towards mechanistic degradation of organic pollutant. *Chemosphere*, 286, 131651. DOI: 10.1016/j.chemosphere.2021.131651.

[13] Franz, S., Perego, D., Marchese, O., Bestetti, M. (2015). Photoelectrochemical advanced oxidation processes on nanostructured TiO_2 catalysts: Decolorization of a textile azo-dye. *Journal of Water Chemistry and Technology*, 37(3), 108–115. DOI: 10.3103/S1063455X15030029.

[14] Zheng, X., Shen, Z.P., Shi, L., Cheng, R., Yuan, D.H. (2017). Photocatalytic membrane reactors (PMRs) in water treatment: Configurations and influencing factors. *Catalysts*, 7(8), 224. DOI: 10.3390/catal7080224.

[15] Yuliwati, E., Ismail, A.F. (2011). Effect of additives concentration on the surface properties and performance of PVDF ultrafiltration membranes for refinery produced wastewater treatment. *Desalination*, 273(1), 226–234. DOI: 10.1016/j.desal.2010.11.023.

[16] Liu, F., Hashim, N.A., Liu, Y., Abed, M.R.M., Li, K. (2011). Progress in the production and modification of PVDF membranes. *Journal of Membrane Science*, 375(1–2), 1–27. DOI: 10.1016/j.memsci.2011.03.014.

[17] Saljoughi, E., Mousavi, S.M. (2012). Preparation and characterization of novel polysulfone nanofiltration membranes for removal of cadmium from contaminated water. *Separation and Purification Technology*, 90, 22–30. DOI: 10.1016/j.seppur.2012.02.008.

[18] Ahmad, A.L., Abdulkarim, A.A., Ooi, B.S., Ismail, S. (2013). Recent development in additives modifications of polyethersulfone membrane for flux enhancement. *Chemical Engineering Journal*, 223, 246–267. DOI: 10.1016/j.cej.2013.02.130.

[19] Lohokare, H.R., Muthu, M.R., Agarwal, G.P., Kharul, U.K. (2008). Effective arsenic removal using polyacrylonitrile-based ultrafiltration (UF) membrane. *Journal of Membrane Science*, 320(1–2), 159–166. DOI: 10.1016/j.memsci.2008.03.068.

[20] Han, Y., Xu, Z., Gao, C. (2013). Ultrathin graphene nanofiltration membrane for water purification. *Advanced Functional Materials*, 23(29), 3693–3700. DOI: 10.1002/adfm.201202601.

[21] Kim, J., Suh, D., Kim, C., Baek, Y., Lee, B., Kim, H.J., Lee, J.C., Yoon, J. (2016). A high-performance and fouling resistant thin-film composite membrane prepared via coating TiO_2 nanoparticles by sol-gel-derived spray method for PRO applications. *Desalination*, 397, 157–164. DOI: 10.1016/j.desal.2016.07.002.

[22] Sokhandan, F., Homayoonfal, M., Davar, F. (2020). Application of zinc oxide and sodium alginate for biofouling mitigation in a membrane bioreactor treating urban wastewater. *Biofouling*, 36(6), 660–678. DOI: 10.1080/08927014.2020.1798934.

[23] Méricq, J.P., Mendret, J., Brosillon, S., Faur, C. (2015). High performance PVDF-TiO_2 membranes for water treatment. *Chemical Engineering Science*, 123, 283–291. DOI: 10.1016/j.ces.2014.10.047.

[24] Nguyen, M.N., Kragl, U., Barke, I., Lange, R., Lund, H., Frank, M., Springer, A., Aladin, V., Corzilius, B., Hollmann, D. (2020). Coagulation using organic carbonates opens up a sustainable route towards regenerated cellulose films. *Communications Chemistry*, 3(1), 116. DOI: 10.1038/s42004-020-00360-7.

[25] Wittmar, A., Thierfeld, H., Köcher, S., Ulbricht, M. (2015). Routes towards catalytically active TiO_2 doped porous cellulose. *RSC Advances*, 5(45), 35866–35873. DOI: 10.1039/c5ra03707g.

[26] Xu, J., Li, G., Li, L. (2008). CeO_2 nanocrystals: Seed-mediated synthesis and size control. *Materials Research Bulletin*, 43(4), 990–995. DOI: 10.1016/j.materresbull.2007.04.019.

[27] Jiang, H., Rinke, P., Scheffler, M. (2012). Electronic properties of lanthanide oxides from the GW perspective. *Physical Review B - Condensed Matter and Materials Physics*, 86(12), 125115. DOI: 10.1103/PhysRevB.86.125115.

[28] Wang, Y., Zhao, J., Wang, T., Li, Y., Li, X., Yin, J., Wang, C. (2016). CO_2 photoreduction with H2O vapor on highly dispersed CeO_2/TiO_2 catalysts: Surface species and their reactivity. *Journal of Catalysis*, 337, 293–302. DOI: 10.1016/j.jcat.2015.12.030.

[29] Majumder, D., Chakraborty, I., Mandal, K., Roy, S. (2019). Facet-Dependent Photodegradation of Methylene Blue Using Pristine CeO_2 Nanostructures. *ACS Omega*, 4(2), 4243–4251. DOI: 10.1021/acsomega.8b03298.